

TWO AIRFOIL SECTIONS DESIGNED FOR LOW REYNOLDS NUMBER

J. H. McMasters
R. H. Nordvik
M. L. Henderson
J. H. Sandvig

Seattle, Washington, USA

Presented at the XVIIth OSTIV Congress
Paderborn, Germany
May 1981

INTRODUCTION

In reference¹, McMasters and Henderson presented an overview of a process by which an airfoil can be tailored to the requirements of a specific application by the use of true inverse viscous flow computational methods. While reference¹ presented a comprehensive overview of this synthesis process, the examples presented were of a preliminary nature demonstrating trends rather than defining specific new airfoil sections.

The present paper is an extension of reference¹ describing in detail two airfoil sections recently designed by this methodology. Both sections were designed to operate at low Reynolds number, are somewhat unconventional, and clearly demonstrate the capabilities of the present synthesis approach. While both sections described are "single element" airfoils (i.e., they possess neither slotted leading or trailing edge high lift devices), the present methodology is fully capable of handling these more complex multi-element cases as well.

The two airfoil sections to be described are:

1. A thick ($t/c = 0.288$) symmetric section specifically designed to operate without significant separation over a limited angle of attack range at Reynolds number from $10^5 \leq Rn \leq 10^6$. This section has been wind tunnel tested and is currently in use for one of its intended purposes.
2. An airfoil intended to solve a rather difficult three design point problem for an ultra-light sailplane application. No test data for this section

presently exists, and all results presented are theoretical.

NOTATION

AR	Aspect ratio = $b/\bar{c} = b^2/S$
b	Wing span (m)
c	Chord (m)
\bar{c}	Average chord - S/b (m)
c_d	Section drag coefficient
C_f	Skin friction coefficient
C_L	Wing lift coefficient = lift/ qS
C_l	Section lift coefficient
C_p	Pressure coefficient = $(p-p_\infty)/q_\infty$
C_m	Section pitching moment coefficient
H	Boundary layer form parameter = δ^*/θ
M	Mach number
p	Static pressure (N/m^2)
q	Dynamic pressure = $1/2 \rho V^2$ (N/m^2)
Rn	Reynolds number = Vc/ν
S	Wing area (m^2)
t	Airfoil thickness (m)
V	Velocity (m/s)
W	Weight (N)
x	Chordwise coordinate
z	Coordinate normal to chord

GREEK SYMBOLS:

- α Angle of attack (degrees)
- δ^* Boundary layer displacement thickness = $\int_0^\infty (1 - \frac{v}{V_\infty}) dz$
- ϵ Section lift-drag ratio = c_l/c_d
- θ Boundary layer momentum thickness = $\int_0^\infty \frac{v}{V_\infty} (1 - \frac{v}{V_\infty}) dz$
- ν Kinematic viscosity ($1.46 \times 10^{-5} \text{ m}^2/\text{s}$ standard sea level)
- ρ Air mass density (1.225 kg/m^3 standard sea level)

SUBSCRIPT:

- ()r recovery point or region
- ()tr transition point or "trip" location
- ()fp fair point
- ()TE trailing edge
- () ∞ free-stream condition
- ()u airfoil upper surface value
- ()d indicates "design condition"

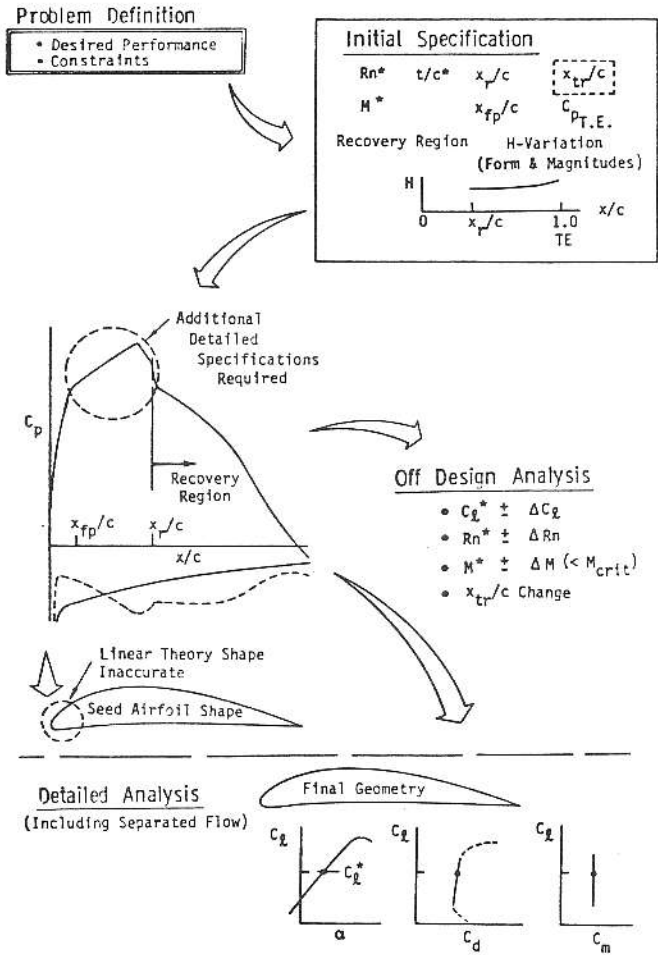


FIGURE 1. GENERAL AIRFOIL DESIGN PROCEDURE

BASIC DESIGN PROCEDURE REVIEW

The basic airfoil design process has been discussed in reference¹ and is shown in broad outline in Figure 1. The crux of this process is the powerful computer program system developed by Henderson, the basic elements of which are described in reference² and reference³. The computer program can both analyze and design two-dimensional multi-element airfoil sections in viscous flow; including the calculation of the effects of large scale flow separation from one or more airfoil elements. This method employs panel method algorithms for potential flow and state-of-the-art integral boundary layer methods for viscous flow computations. The overall program system also incorporates an inverse boundary layer method for the design and evaluation of desirable pressure distributions for input to the design mode of the program. The inverse

boundary layer method (ref.²) is a valuable tool in its own right and when coupled with the panel method design capabilities of the overall program gives the designer a powerful and flexible tool for the optimization of arbitrary single and multi-element airfoils. For brevity in the subsequent discussion, the elements of the computer system will be identified as follows:

- Program X - The inverse boundary layer method used for pressure distribution design and parametric evaluations.
- Program Y - An auxiliary airfoil design program, based on linear theory, used to extract a preliminary "seed" airfoil geometry from Program X pressure distributions.

Program Z - The full panel method analysis (Program Za) and design (Program Zd) program used to extract the exact airfoil geometry and analyze its performance (including the effects of separated flow).

Using these tools, the basic design process consists of the following steps:

1. Using Program X, and the linear airfoil design Program Y, perform a parametric analysis of various viscous flow pressure distributions to determine preliminary performance and section geometry.
2. Derive a "final" viscous flow pressure distribution (using Program X) which provides:
 - a. Orderly transition of the initial laminar boundary layer to a turbulent one ahead of the selected pressure recovery region over the operating Reynolds number and angle of attack range.
 - b. Little or no separation. (When separation does begin it is usually desired that it should progress forward gradually from the trailing edge of the section over the desired operating Reynolds number and angle of attack range.)
3. From the pressure distribution derived in step 2 above, extract a preliminary linear design airfoil shape (Program Y). This resulting (seed) shape is a first approximation of the final airfoil contour plus its boundary layer at the design Reynolds number and angle of attack.
4. With the desired pressure distribution and seed airfoil defined, using Program Z, generate the exact airfoil geometry with the boundary layer removed.
5. As the final step, the exact airfoil geometry is analyzed using Program Za at various values of Reynolds number and angle of attack, performance predictions are made and compliance with the initial design specification is verified.

This overall procedure, shown schematically in Figure 2, is the basis for the design of the two airfoil sections discussed in this paper.

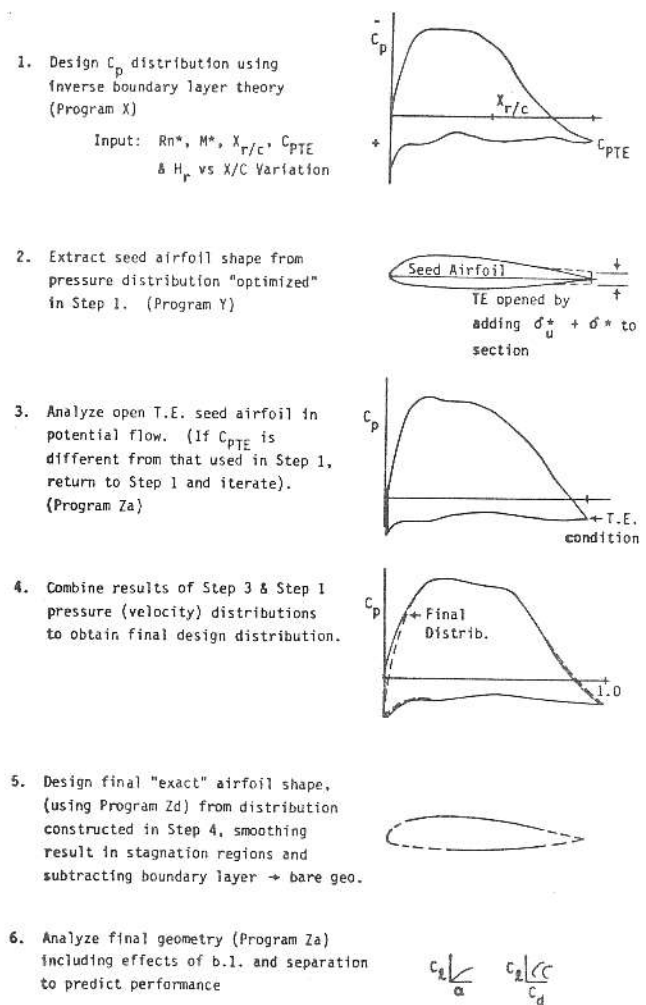


FIGURE 2. DETAIL AIRFOIL DESIGN PROCEDURE

A THICK SYMMETRIC AIRFOIL

Design Objectives

The basic objective of this design effort was to devise a symmetric airfoil section of maximum practical thickness. The intended application was to a long, small chord (25-50 mm) strut to be used to support flow field sensors in low-speed wind tunnel ducts. Thus, to provide adequate mechanical stiffness a thick section was desired, and at the same time it was desired that the strut section disturb the flow being investigated as little as possible. The resulting design specifications for the airfoil section was:

- Maximum practical thickness/chord ratio
- Little or no flow separation over the range of operating conditions

- Operating angle of attack range of $\pm 3^\circ$ to 5°
- Operating Reynolds number range from 10^5 to 10^6
- Design Mach number 0.1

STRUT SECTION DESIGN

For a symmetric section at zero angle of attack the pressure distribution that a non-separating boundary layer can support at a given Reynolds number will be that produced solely due to thickness. If one constructs this design condition pressure distribution carefully and with sufficient conservatism in a viscous flow, a section of rather substantial thickness can result, while still providing sufficient margin to behave well when operated over the desired angle of attack range. The ultimate values of thickness/chord ratio obtainable for a strut section will depend on:

- The operating Reynolds number range
- The desired angle of attack range without significant separation
- The desired level of insensitivity to freestream flow disturbances and surface irregularities.

For general airfoils, there are other factors (e.g., stall behavior, pitching moment) of importance; however, the above short list is sufficient for the strut case.

It must always be kept in mind that the boundary layer characteristics will ultimately determine the performance of the section in every way and the range of Reynolds number of interest in the present problem presents some difficulties in this respect. At lower Reynolds number (10^5) the problem is not to maintain laminar flow, but rather to get rid of it in an orderly fashion and assure transition to a thin turbulent boundary layer ahead of the point where the pressure recovery will begin over the full desired range of Reynolds number and angle of attack.

For clarification of this factor in the present problem, one can refer to the general (simplified) pressure distribution shown in Figure 3, wherein several important parameters in the design problem are defined. At the design point (zero angle of attack) the pressure distribution consists of:

1. An initial pressure drop to some "low" (relative to freestream) value near the nose of the section.

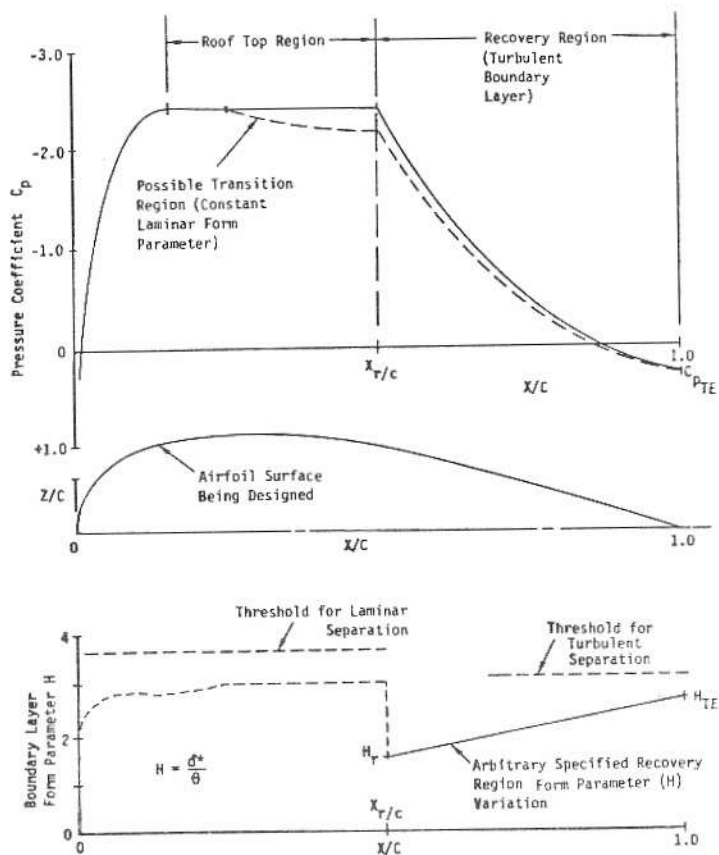


FIGURE 3. TYPICAL PRESSURE DISTRIBUTION ARCHITECTURE

2. A "roof top" region of peak pressure, the chordwise gradient of which is determined by the degree of resistance to transition to turbulent flow desired.
3. A final recovery region wherein the pressure rises again to near free-stream conditions at the trailing edge. Avoidance of separation demands that the recovery be accomplished with a healthy turbulent boundary layer.

In the present problem, at the design angle of attack (0°) and Reynolds number, the feasible pressure distribution is dependent on the recovery capability of the unseparated turbulent boundary layer, which in turn dictates the maximum level of peak "roof top" pressure, which in turn correlates directly with the maximum allowable thickness of the strut section. That is, the more negative the allowable roof-top pressure coefficient level, the greater the achievable thickness of the strut.

In the present problem, the magnitude of the drag is unimportant (i.e., we merely wish to avoid the flow disturbances caused by separation). Thus, achievement of an extensive run of laminar flow is not a direct objective, and the distribution of thickness is not fundamental. There is, therefore, wide latitude in the selection of "optimum" recovery point and input recovery region boundary layer characteristics. The possibilities here are extensive and are elaborated in detail in refs. 1 and 2. The factors of greatest importance are:

1. Assurance that over the operating Reynolds number range the point of natural transition neither moves aft of the point where the pressure recovery is to begin (important at $R_n = 10^5$ to avoid formation of a long laminar separation bubble); nor that the transition point moves so far forward that the subsequent boundary layer is too sluggish to accomplish the necessary recovery without separating.
2. The recovery region boundary layer characteristics specified as design inputs (see Fig. 1) are sufficiently conservative to:
 - a. Provide a minimum of separation, once separation begins, coupled with:
 - b. The lowest roof top pressure level possible without separation in order to achieve "large" thickness values with:
 - c. Enough latitude to allow angle of attack excursions without significant separation.

Results

In view of the wide range of possible design input parameters (e.g., recovery point location, recovery region boundary layer form parameter variation) and the under-constrained nature of the original design specification; coupled with past experience with use of the inverse boundary layer design program, the following ground rules and assumptions were set down to further guide the design effort:

1. The resulting design should meet the design objectives conservatively (i.e., no attempt would be made to find the section of theoretical absolute maximum thickness). Enough is sufficient.
2. The resulting cross-section geometry should not be unreasonably sensitive to surface imperfections or demand unreasonable manufacturing tolerances,

particularly when built with small chordwise dimensions.

3. A linear variation in boundary layer recovery region form parameter (H) was selected as a reasonable compromise between:
 - a. Achievable thickness
 - b. Benevolent separation progression
 - c. Reasonable resulting geometry

With these additional constraints in hand, a parametric analysis of achievable thickness versus:

1. Recovery point location ($0.35 \leq x_r/C \leq 0.6$)
2. Trailing edge form parameter value ($H_r < H_{TE} < 3$)
3. Pressure distribution "roof top" shape

was conducted with Reynolds number varied between 10^5 and 10^6 . The influence of changes of angle of attack for each significant case was also evaluated.

From this parametric analysis, it was determined that:

1. The optimum recovery point for the specified Reynolds number range should be at approximately 50% of the chord.
2. The realistic value of trailing edge pressure coefficient (a very powerful factor in the problem) was about +0.3.
3. A very long "instability" ramp needed to be built into the roof top portion of the pressure distribution, to assure orderly natural transition over the whole range of Reynolds number.
4. The possible range of thickness chord ratios for the proposed strut varied from 20% to about 38%, with the high value apparently approaching a theoretical limit within the low end of the Reynolds number range considered. The 38% thick strut would, however, have virtually no resistance to massive separation at angles of attack other than zero.
5. The linear recovery region form parameter (H) variation appeared quite satisfactory both with respect to strut performance and resulting geometric shape (i.e., the strut section has only a very slight cusp or concavity in the recovery region).

As a consequence of these parametric analysis results, a final proposed strut

configuration was derived. The strut was 28.8% thick and operated satisfactorily over the ranges $10^5 \leq R_n \leq 10^6$ and $-3^\circ \leq \alpha \leq +3^\circ$ without separation and $-5^\circ \leq \alpha \leq +5^\circ$ with very minor trailing edge separation - based on purely theoretical predictions. The resulting geometry and its coordinates are shown in Fig. 4 and Table 1.

x/c	(±) y/c	x/c	(±) y/c
0.0	0.0	.3416	.1423
.0004	.0047	.3814	.1395
.0010	.0121	.4212	.1357
.0017	.0195	.4610	.1309
.0040	.0294	.4808	.1279
.0077	.0390	.5008	.1246
.0122	.0484	.5205	.1210
.0176	.0581	.5407	.1169
.0235	.0668	.5804	.1081
.0337	.0782	.6202	.0986
.0436	.0876	.6600	.0889
.0532	.0951	.7001	.0788
.0628	.1014	.7400	.0687
.0824	.1115	.7800	.0587
.1025	.1194	.8196	.0488
.1227	.1257	.8394	.0440
.1428	.1308	.8593	.0392
.1626	.1349	.8792	.0343
.1823	.1382	.8991	.0294
.2022	.1406	.9188	.0247
.2221	.1423	.9390	.0194
.2620	.1440	.9589	.0140
.3018	.1438	.9788	.0083
		.9988	.0021

TABLE 1. STREAMLINED STRUT ORDINATES

Wind Tunnel Test Results

The geometry and predicted flow physics which resulted from the design effort were judged sufficiently interesting to warrant conducting a well instrumented wind tunnel test. These tests were conducted in the 5' x 8' (1.5 x 2.4 meter) Boeing Research Wind Tunnel (BRWT) at the end of 1979.

The model tested consisted of a 0.3m (chord) by 1.5m (span) aluminum version of the final configuration which was to be manufactured in 25-50mm chord in its intended applications. A high manufacturing tolerance level was specified over the center portion of the model which was instrumented with 46 static pressure tags as shown in Fig. 4. Lift and drag data were obtained from both force balance measurements and pressure integration (chord wise for normal force, and wake survey for drag). Provision was made for wind tunnel test section wall blowing to assure full two-dimensionality of flow, although in the event this proved unnecessary since this was not a high lift test. All data was collected without blowing. A novel feature of the data acquisition was the use of the Hewlett-Packard data system developed by the Boeing Wind Tunnel Testing Development Group which gave high quality data - near "on line" - of normal force, drag and pressure distributions. Data collected consisted of complete pressure distributions (chordwise and wake profiles) for the "smooth" model over the range $-10^\circ \leq \alpha \leq +20^\circ$ to -30° (depending on stall angle of attack) for four values of dynamic pressure:

- q = 2 psf $R_n = 0.25 \times 10^6$
- q = 5 psf $R_n = 0.4 \times 10^6$
- q = 15 psf $R_n = 0.7 \times 10^6$
- q = 35 psf $R_n = 10^6$

These values covered the range of design conditions to within the limitations (low g values) of the BRWT facility.

In addition to the "smooth" model tests, tests were conducted at q = 35 psf and q = 5 psf with a trip (made of glass micro beads) at 8% x/c on the upper surface designed to be effective at $\alpha = +10^\circ$ at q = 35 psf. The trip effectiveness was verified by fluorene sublimation. Two-demensionality of the flow was assured by flow visualization (china clay, fluorescent oil flow) and by wake traverse at four spanwise stations over the angle of attack range of the experiment at q = 5 psf and q = 35 psf.

Some results of the wind tunnel test are shown in Figures 5 through 7. Fig. 5 shows the excellent agreement between theoretical (design) and experimental zero angle of attack pressure distributions. Also shown in Fig. 5 is the comparison between measured and predicted separation point migration with angle of attack. It may be noted that the strut section performed substantially better than predicted (or required) at all Reynolds numbers tested.

Fig. 6 shows measured lift and drag characteristics, while Fig. 7 shows some of the flow visualization results obtained during the test.

The results of the wind tunnel tests showed that the design was far too conservative and subsequently, the empiricism involved in the transition prediction portion of the computer program was re-evaluated. The need to re-evaluate the empiricism in the boundary layer computational methods was expected, and the collection of data for this purpose was an objective of the test. In any event, the present strut section in its final configuration (40mm chord) has been operated with success in several wind tunnels.

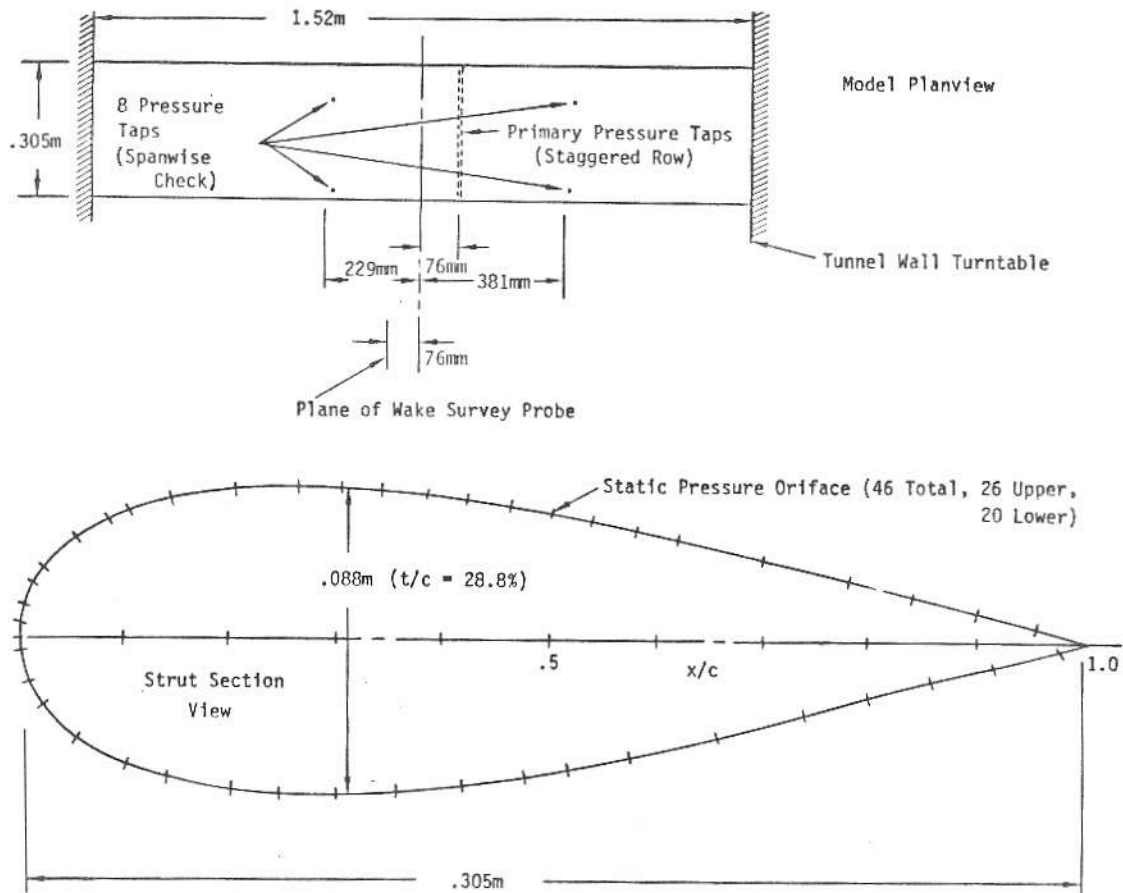


FIGURE 4. CONFIGURATION OF THICK STREAMLINED STRUT AS TESTED

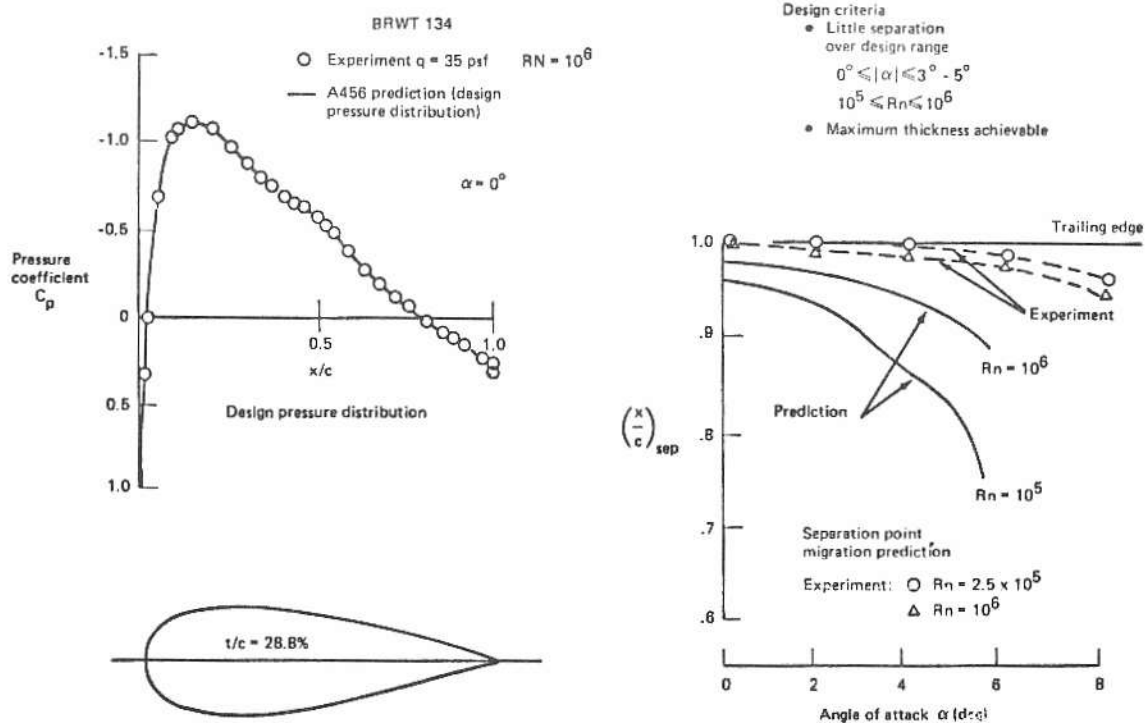


FIGURE 5. THICK STRUT TEST/THEORY COMPARISON

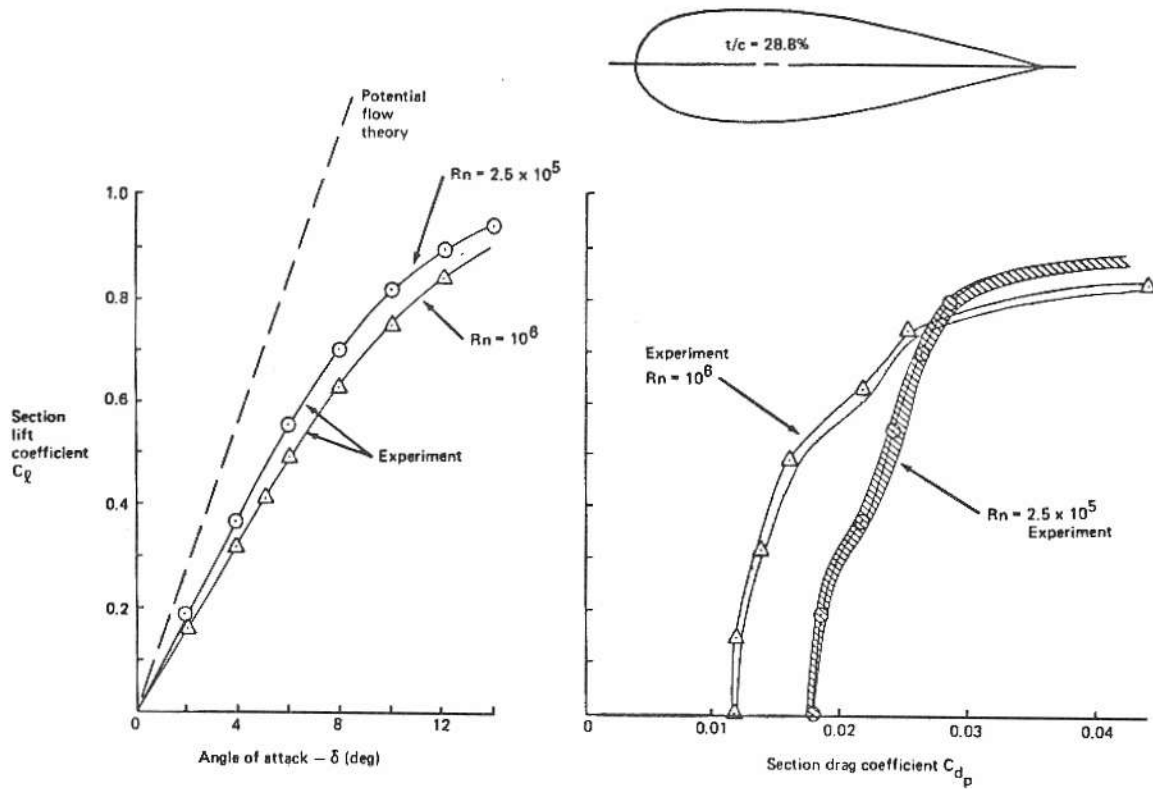
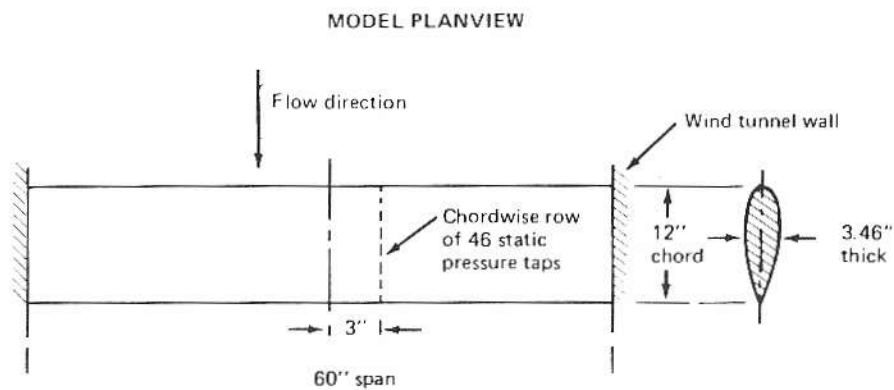


FIGURE 6. THICK STREAMLINED STRUT PERFORMANCE (WIND TUNNEL TEST)



FLUORESCENT KEROSENE FLOW VISUALIZATION

$q = 35 \text{ psf}$

$R_n = 1 \times 10^6$

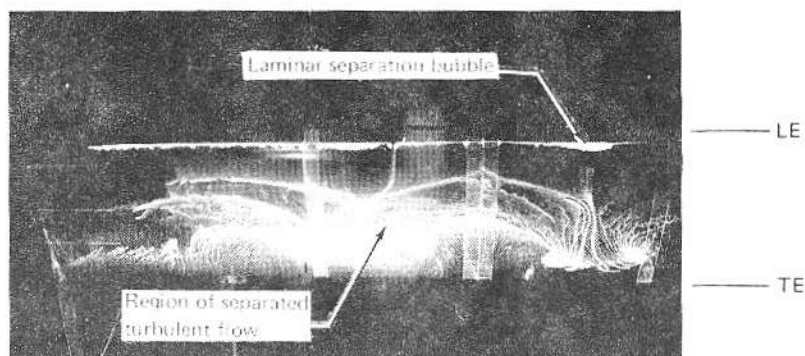
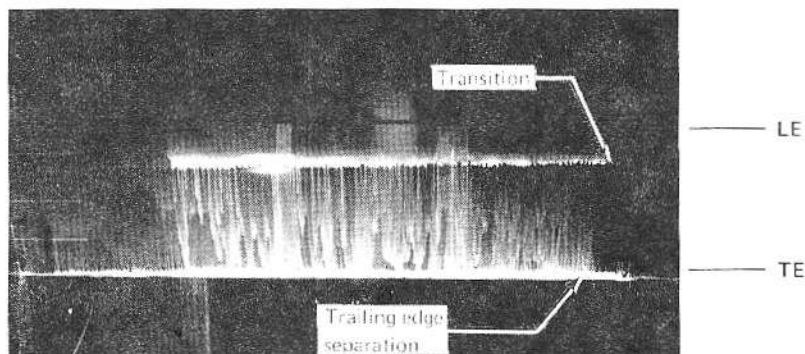


FIGURE 7. THICK STREAMLINED STRUT TEST CONFIGURATION
AND FLUORESCENT KEROSENE FLOW VISUALIZATION

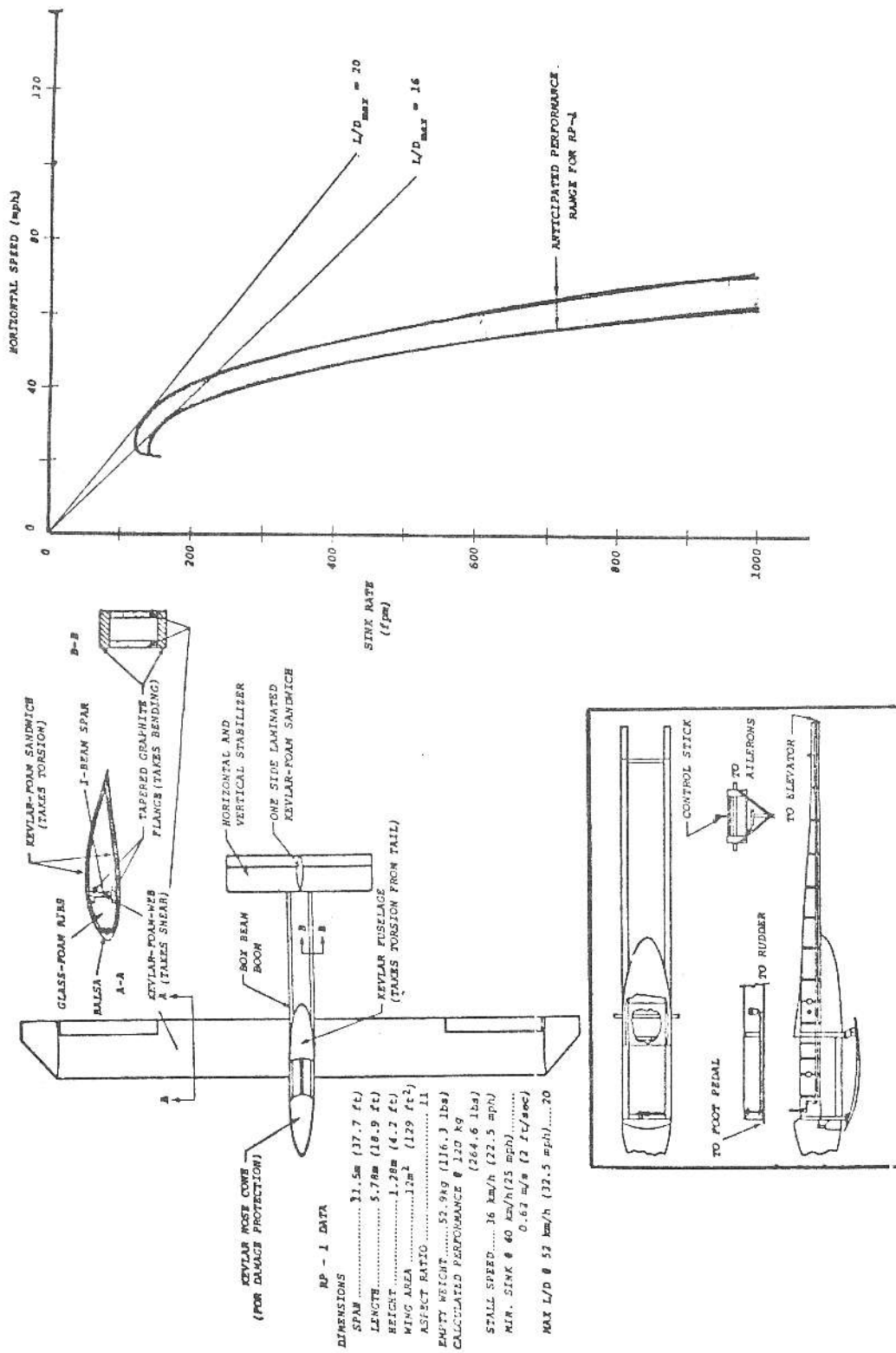


FIGURE 8. RP-1 CAPGLIDE ULTRALIGHT SAILPLANE

A NOVEL ULTRALIGHT GLIDER AIRFOIL

Background

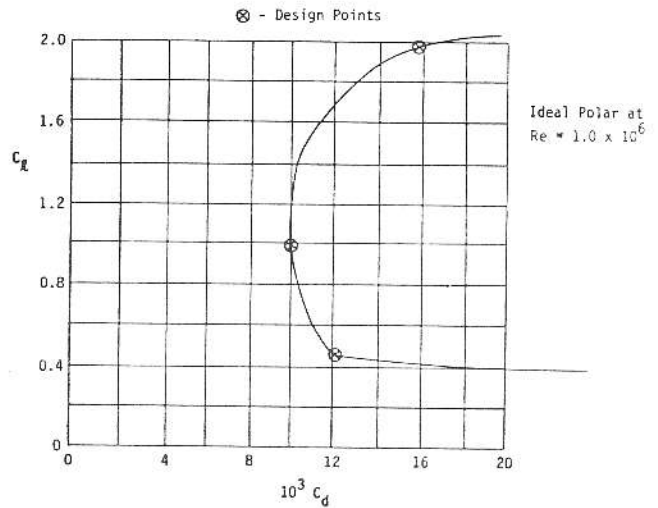
The object of this exercise was to design an airfoil specifically tailored to the performance requirements of an ultralight sailplane being designed at Rensselaer Polytechnic Institute (RPI) in Troy, New York. The initial version of the glider (which has now flown) is shown in Fig. 8. In its initial version (the RP-1, ref. 4), the glider was constructed almost entirely of advanced composite materials and utilized the Wortmann FX 63-137 airfoil, originally designed for human powered aircraft applications. While the overall performance of the FX 63-137 is outstanding, its two liabilities in the present application are the high negative pitching moment (which creates problems of high torsional shear loads on the RPI structural configuration) and the extremely thin, cusped trailing edge geometry which is difficult to manufacture with the accuracy and stiffness necessary to maintain the sections aerodynamic performance. It was hoped that an alternative section of similar performance, but of improved structural form and reduced pitching moment, could be devised by the previously described airfoil synthesis procedure.

Design Specification

The original drag polar and design constraints specified to the authors by RPI is shown in Fig. 9. A more detailed evaluation of the actual variation in average airfoil section operating Reynolds number with lift

coefficient is shown in Fig. 10. The final agreed upon design specification (labeled RP-X) together with design priorities is shown in Table 2.

- Other Constraints:
- Thickness $\geq 12\%$
 - Pitching Moment $|C_m| \leq 0.05$
 - Gentle Stall



Note: The Original Specification Did Not Properly Account For Reynolds Number Variation With Lift Coefficient Values For an Aircraft of Fixed Weight and Geometry.

FIGURE 9. PRELIMINARY DESIRED DRAG POLAR SPECIFICATION

Table 2. Airfoil Design Specification

Design Parameter	RP-1 FX 63-137 Airfoil	RP-X Airfoil Specification	RP-X Design Priority
1. c_d at $c_l = 1.0$ and $Rn = 1 \times 10^6$	≈ 0.009	0.01	1
2. $c_{l_{max}}$ at $Rn = 6 \times 10^5$	1.78	2.0	1
3. Lift coefficient for onset of low-lift drag rise at $Rn = 1.5 \times 10^6$	0.5	0.4	3
4. $c_m \geq$ at $0.4 \leq c_l \leq 1.0$	-0.25	-0.05	1
5. Stall Characteristics	Gentle	Gentle	2
6. Thickness/Chord $>$ (with t/c_{max} at $\bar{x}/c \geq$)	13.7 $x/c = 0.4$	12 at $x/c \geq 0.30$	2

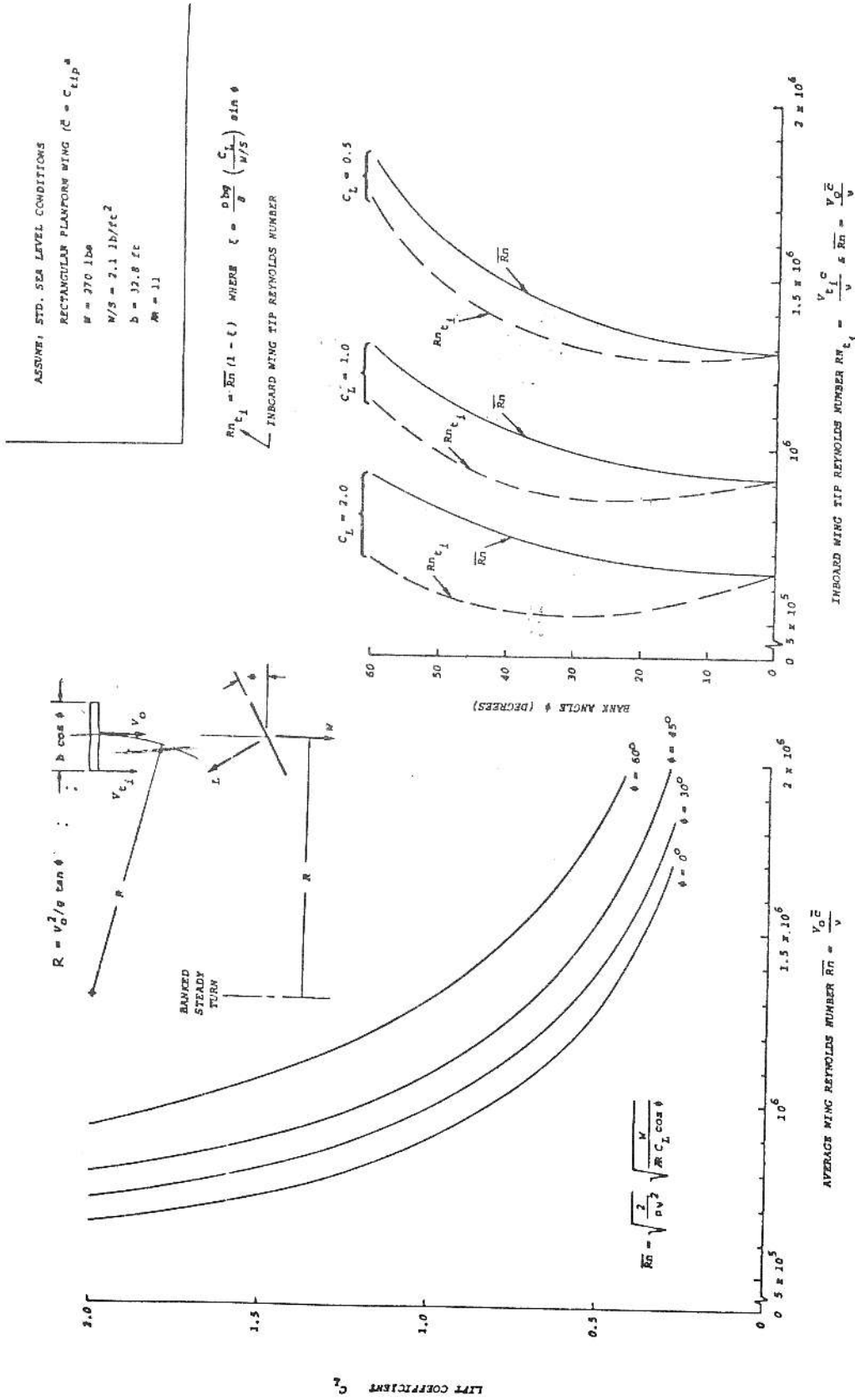


FIGURE 10. DESIGN VALUES OF REYNOLDS NUMBER VERSUS AVERAGE SECTION LIFT COEFFICIENT

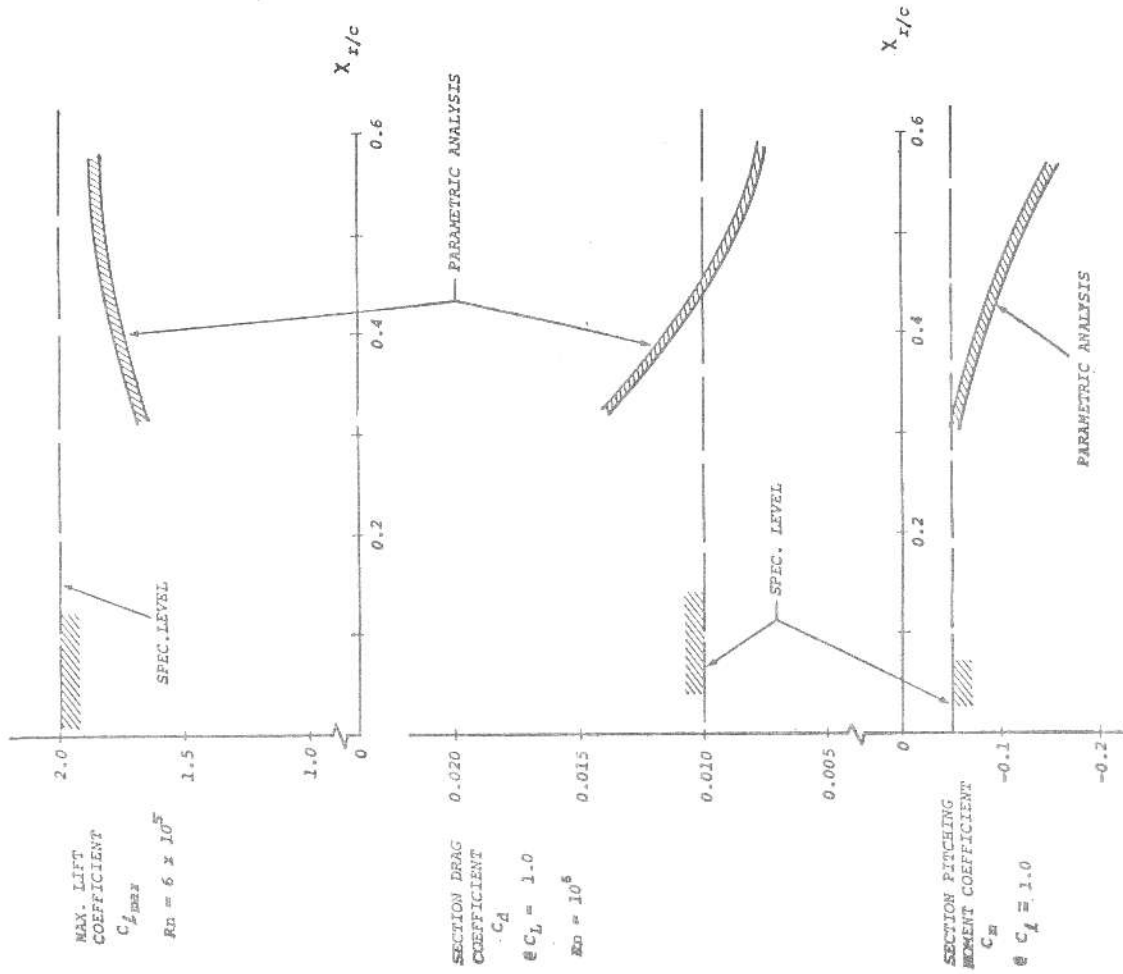


FIGURE 12. SPECIFIC RESULTS OF AIRFOIL PARAMETRIC ANALYSIS

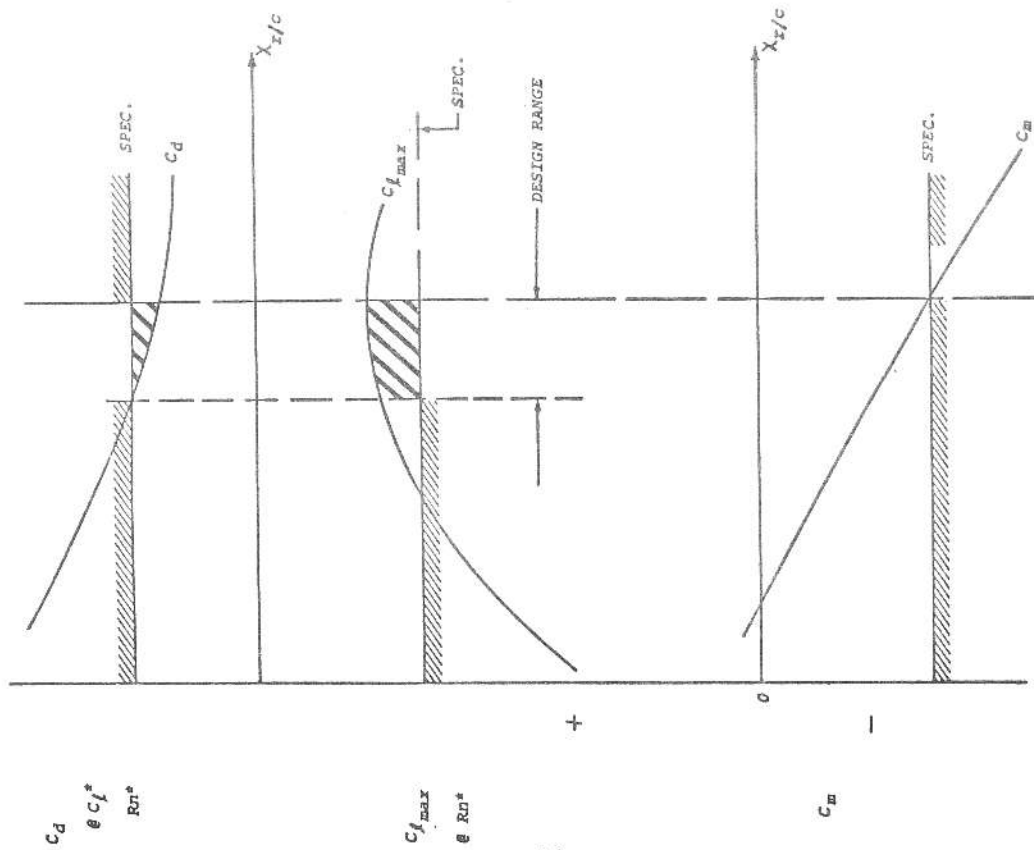


FIGURE 11. CONCEPTUAL AIRFOIL PARAMETRIC ANALYSIS RESULTS

Initial Parametric Analysis

With a more-or-less well defined design specification in hand, the next step was to perform a parametric analysis of the problem. In this case, Program X was used to establish:

1. Trades between lift, drag and pitching moment at the critical design points as a function of the physical characteristics of the flow as represented by Reynolds number, pressure distribution architecture, trailing edge pressure coefficient and the point at which the flow begins its (turbulent) recovery to free-stream conditions (i.e., the recovery point location) on the surface of the airfoil being designed.
2. The level of performance achievable at each design point to establish whether the performance objectives could, in fact, be met as specified.
3. A baseline design pressure distribution and initial airfoil geometry suitable for subsequent detailed analysis and design using Program Z.

Conceptually, the result of such a parametric analysis would result in the sort of data sketched in Fig. 11. The actual results obtained in the detailed parametric analysis are shown in Fig. 12. The constraints could not be met while simultaneously meeting the basic performance objectives with a single fixed geometry airfoil.

A Variable Thickness and Camber Airfoil

Having reached an apparent impasse in the design effort, based on results of the initial parametric analysis, the requirements were re-evaluated. The problem at this point reduced to the following considerations:

1. The upper surface contour was critical in meeting the low Reynolds number, high lift requirements ($c_{l_{max}}$ and gentle stall), and therefore must be optimized for this condition.
2. To get close to the maximum lift coefficient desired at the Reynolds number of 6×10^5 , the lower (under) surface of the airfoil must produce a substantial portion (15-20%) of the net lift on the section, and this resulted in a requirement (ideally) for an under cambered section whose minimum thickness was limited mainly by the thickness/chord constraint.
3. The resulting under cambered section,

optimized for high lift, had higher than desired pitching moments at low lift, was quite thin and, most importantly, suffered severe under surface separation when operated at low-to-moderate angles of attack (and lift coefficient levels) at any Reynolds number. Thus, the "high-speed" drag specification could not be met.

4. The way to solve the drag problem was to combine the optimized high lift upper surface with a lower surface which was more nearly optimum (in a drag sense) at lower lift coefficient levels. To do this required creating an under surface pressure distribution which was more favorable to maintenance of a substantial run of laminar flow at low-to-moderate lift coefficients without separation at those conditions. Such a lower surface pressure distribution in turn generated a requirement for a convex under surface contour with the degree of convexity roughly proportional to the increasing extent of the low drag range of lift coefficient desired. Thus, the wider the "low-drag" range, the thicker the section became, with a concomitant gradual increase in minimum drag coefficient, and loss in maximum lift coefficient capability.
5. The maximum lift and minimum drag performance was strongly influenced by the extent of laminar flow which could be sustained on both surfaces of the section. Thus, performance would be improved in both lift and drag if the pressure recovery point could be moved aft on the section (thus distributing the main lift loading over a greater extent of the chord), provided that the subsequent transition to turbulent flow could be accomplished in a controlled and reliable fashion and did not result in either the upper or lower surface boundary layers separating. However, as the recovery points moved aft, the pitching moment of the section became more strongly nose-down. It further turned out that for a given upper surface recovery point location, the under cambered (high lift) section would have more nose-down pitching moment than the thick (low drag at lower lift) section due to the contribution of the lower surface loading distribution in each case.

6. A gentle stall break would be exhibited by sections on which the separation point moved slowly forward from the trailing edge as angle of attack was increased. As more and more high lift capability was demanded of a section on which the bulk of the loading must occur on the forward portion of the section (e.g., to limit pitching moment), it became increasingly difficult to restrain the rapid forward migration of the separation point and the consequent abruptness of the stall.

This was the aerodynamic story presented to the (structures oriented) members of the RPI faculty involved in the project.

In the ensuing discussion of the aerodynamic pros and cons of the airfoil performance specification, the following clarifications on the specification came to light:

1. While the lift and drag characteristics specified have obvious size/performance consequences, and the minimum thickness/chord requirement had obvious structural and weight consequences, the pitching moment requirement was imposed for structural rather than aerodynamic/flight control reasons. The desire was mainly to limit torsional loads on the wing structure itself and was based upon analysis of the particular structural materials and techniques to be used in the proposed machine.
2. The wing of the proposed RP-X glider was to be made up of a spar with carbon fiber caps to carry bending loads and a foam/fiber glass shear web. Epoxied to this spar were foam/fiber glass ribs; the whole structure was then to be covered with large panels of Kevlar/foam skin. Each single piece skin panel was flexible and covered the entire upper or lower semispan of the rectangular planform wing. If need arose, the Kevlar/foam wing skins could be replaced with carbon fiber/foam panels, without weight penalty. It was the allowable shear loads under torsion between the skins and the substructure which limited the pitching moment of the airfoil, and these loads in turn were dominant at "high speed" (low lift coefficient) conditions. Somewhat higher moments might be allowable at low speed/high lift conditions if the wing was designed for high speed conditions.
3. From RPI's point of view, an airfoil much thicker than the specified minimum

structural depth of 12% was undesirable. The reason for this bizarre situation was that the dominant mode of failure was likely buckling of the shear web in the spar. Since, with the use of the carbon fiber, adequate loads could be carried with a wing of about 12% thickness with minimum weight, increase in thickness beyond this point meant an increase in shear web depth with a consequent requirement to add structure (and weight) to stabilize the minimum gage web against buckling.

4. For manufacturing simplicity a constant chord wing without twist or change of airfoil across the span was selected. With such a planform, wing stall characteristics could be sufficiently benign, even if section stall characteristics were only less than vicious. Thus an airfoil with a more abrupt stall characteristic than at first thought, would be acceptable.

When all of these aerodynamic and structural considerations were combined, it took only a mild leap of imagination to come up with the concept of a variable thickness and camber wing - and the previous pieces of a rather vexing puzzle began to rapidly fall into place.

The bases of the final concept (shown in Fig. 13) were as follows:

Structure - The wing (and its constituent airfoils) would be built in the same fashion as originally envisioned (with roughly 12% thickness) except that the lower surface wing skins would be connected to the internal structure only at the leading and trailing edges of the wing. Thus the highly loaded upper skin, the spar and the ribs would be fixed structure, with the lightly loaded lower skin allowed freedom to flex or "oil can" from a "thick" to a "thin" airfoil configuration. Depending on required stiffness characteristics, the lower skin panel would be either Kevlar or carbon fiber.

High Lift Aerodynamics - The airfoil contour would be optimized to produce the maximum lift at the design Reynolds number of 6×10^5 consistent with the following constraints:

1. The pitching moment should be as low as possible.
2. The stall break should be less than violent.
3. Maximum thickness of 12% at approximately 30% of the chord.
4. Good off design lift characteristics.

Specifically, near the design point maximum lift performance should be maintained down to Reynolds numbers as low as 3×10^5 to avoid inboard wing tip stalls in low speed banked turns.

5. The airfoil under surface shape in the high lift case should be compatible with the "oil can" distortion to the high speed, low drag configuration.

High Speed Aerodynamics - The upper surface contour of the airfoil previously optimized for high lift would be combined with a new lower surface contour to meet both the drag and moment requirements at low-to-moderate lift coefficient levels. There would be no constraint on the allowable thickness of the sections other than those imposed by the above requirements and the need for the new surface to be structurally and aerodynamically compatible with the low speed, high lift lower surface (i.e., the trailing edge pressures must match).

Other Considerations - A question arose regarding actuation of this system and its possible advantage or disadvantage relative to merely fitting the airfoil with a simple hinged flap. With regard to the first question it turns out that, fortuitously, the pressure loadings (see Fig. 17) on the lower surface at the various design conditions are favorable to maintenance of that surface in its desired position. That is, in the high-lift mode, the pressure loading is positive on the under surface, thus holding it against the under (fixed) structure. In the low lift (thick) configuration, the middle portion of the under surface is subjected to a suction loading, thus stabilizing the surface in that configuration. It is therefore possible to contemplate a system which might actuate automatically as a function only of angle of attack. To avoid the possibility of asymmetric "snap through" from one position to the other, however, it seems necessary to place actuation under the positive control of the pilot. Given the airloads on the surface, a simple cam/level mechanism could be incorporated which should operate with minimum actuation loads.

Regarding the question of the proposed system vis-a-vis a more conventional simple hinge flap, it should be noted that the proposed system acts as little more than a very large chord, camber changing flap with very modest deflection capability. Based on tests with structural samples of the system (conducted at RPI) it is the authors present view that the proposed system is probably lighter, simpler and at least as effective as a simple hinged flap for this particular

type of application. Contemplate the secondary load carrying structure necessary to support a flap hinge and the small physical dimensions of the flap parts themselves in the alternative approach.

Final Design Results

With the concept for the variable thickness and camber airfoil clearly in mind, and the results of the Program X parametric analysis in hand, it was possible to complete the design exercise using Program Z in both its design and analysis modes as previously outlined. The final resulting airfoil contours are shown in Fig. 13 and a summary of the approximate compliance of the final design with the original specification is listed in Table 3. Table 4 lists the coordinates of the sections.

To complete the comparison of the design effort results with the specification and the performance of existing similar sections, the series of Figures 14 through 18 are presented. While these figures show that the Boeing section is inferior to several existing sections at any single design point, its performance is superior in an overall sense, particularly in view of the difficult constraints on the problem. Necessary wind tunnel testing of this section to validate the theoretical design results has not been conducted, and the reader is cautioned that such data should be in hand before the sections are used in an actual construction project.

REFERENCES

- ¹McMasters, J.H. and Henderson, M.L., "Low-Speed Single-Element Airfoil Synthesis," *Science and Technology of Low Speed and Motorless Flight*, NASA CP 2085, Pt. 1, 1979. Supplemented version published in *Technical Soaring*, Vol. VI, No. 2, December 1980.
- ²Henderson, M.L., "Inverse Boundary Layer Technique for Airfoil Design," *Advanced Technology Airfoil Research*, NASA CP 2045, Vol. 1, Pt. 1, March 1979.
- ³Henderson, M.L., "A Solution to the 2-D Separated Wake Modeling Problem and Its Use to Predict Maximum Section Lift Coefficient of Arbitrary Airfoil Sections," AIAA Paper No. 78-156, January 1978.
- ⁴Helwig, H.G., "CAPGLIDE and the RP-1," *Soaring*, February 1980, pp. 22-25.

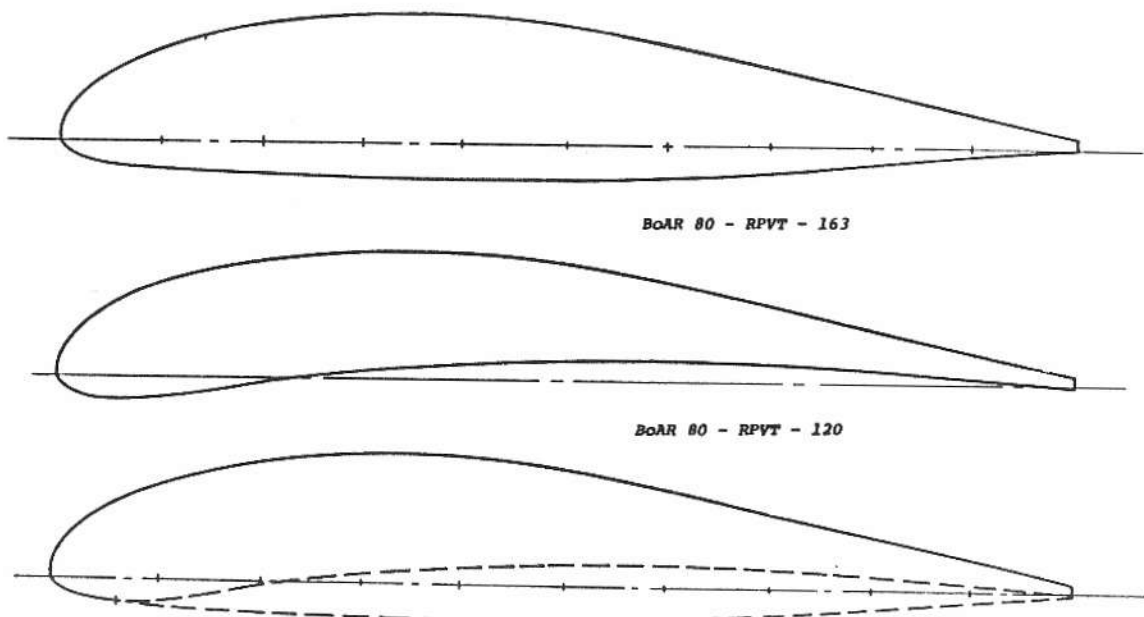
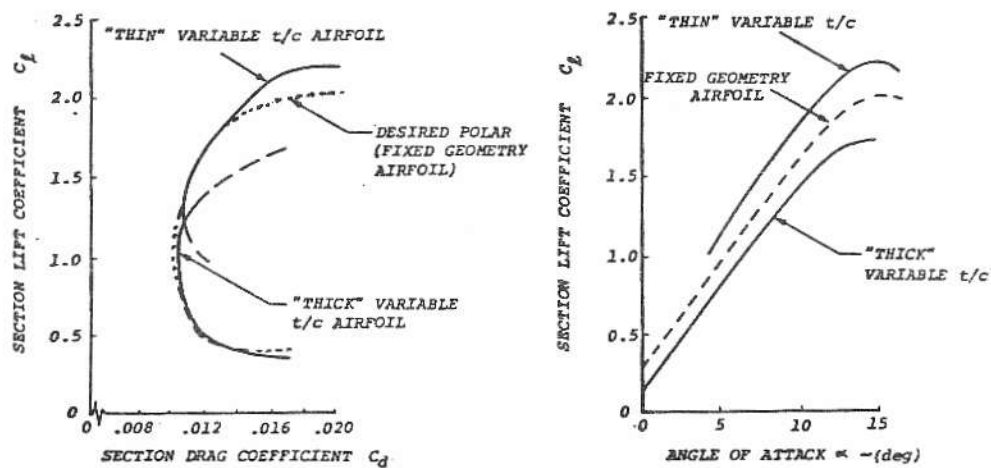


FIGURE 13b. FINAL VARIABLE THICKNESS AIRFOIL CONTOURS



VARIABLE THICKNESS AND CAMBER AIRFOIL

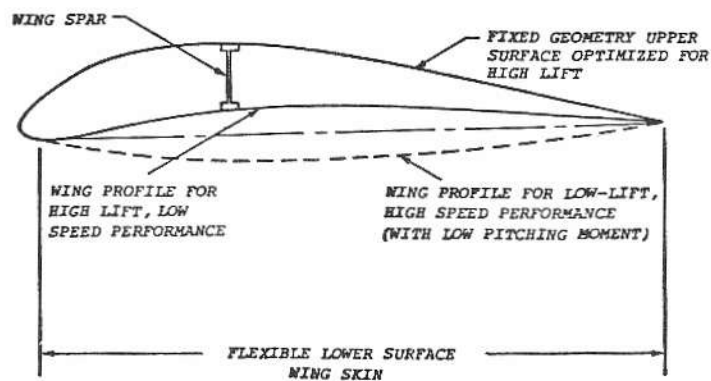


FIGURE 13a. VARIABLE THICKNESS AND CAMBER AIRFOIL CONCEPT

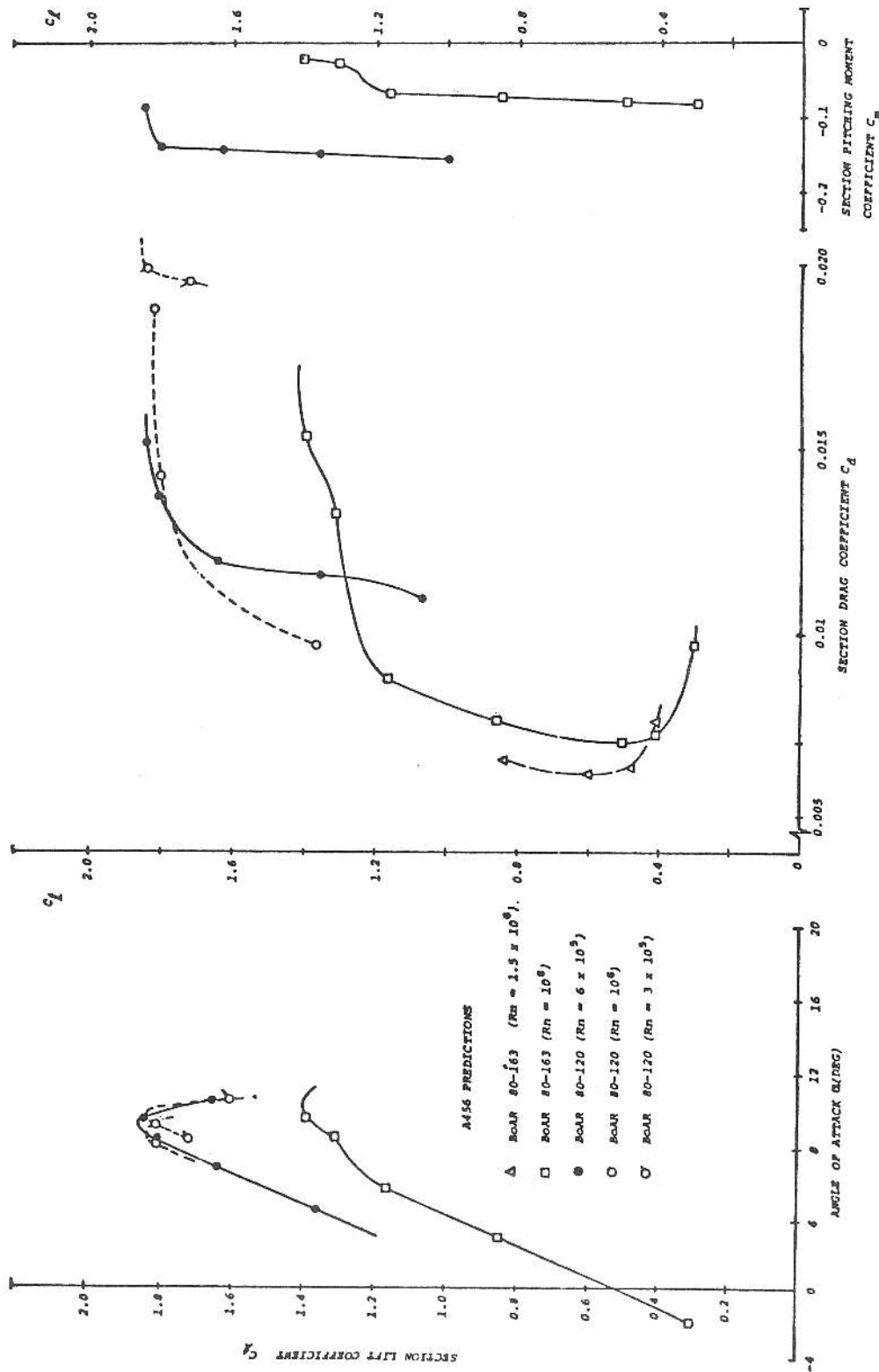


FIGURE 14. FINAL PREDICTED PERFORMANCE OF THE VARIABLE THICKNESS AIRFOILS

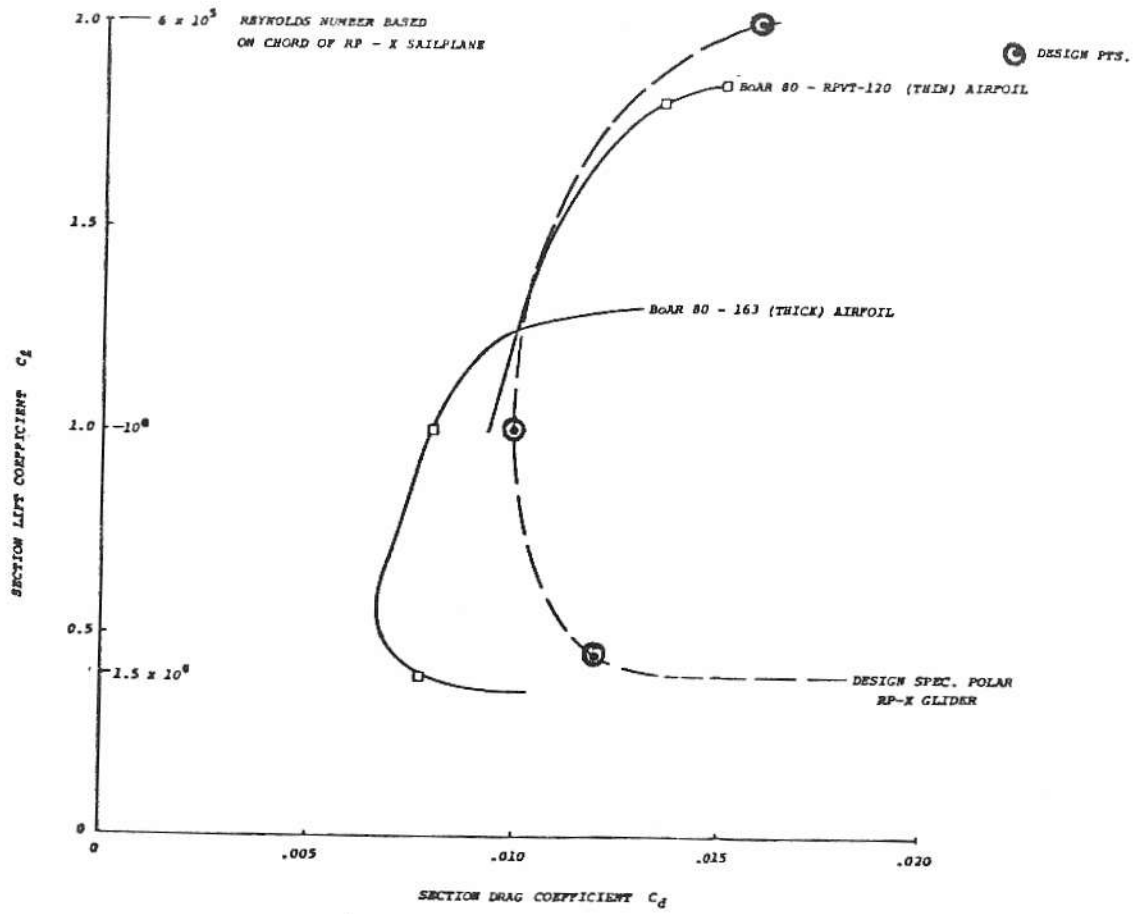


FIGURE 15. COMPARISON BETWEEN DESIGN SPECIFICATION AND FINAL DESIGN AIRFOIL PERFORMANCE

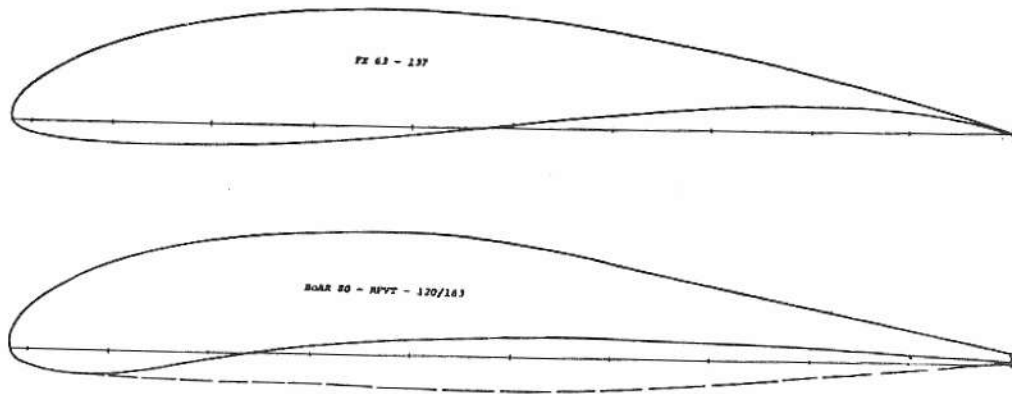


FIGURE 18. COMPARISON BETWEEN FX 63 - 137 AND BoAR AIRFOILS

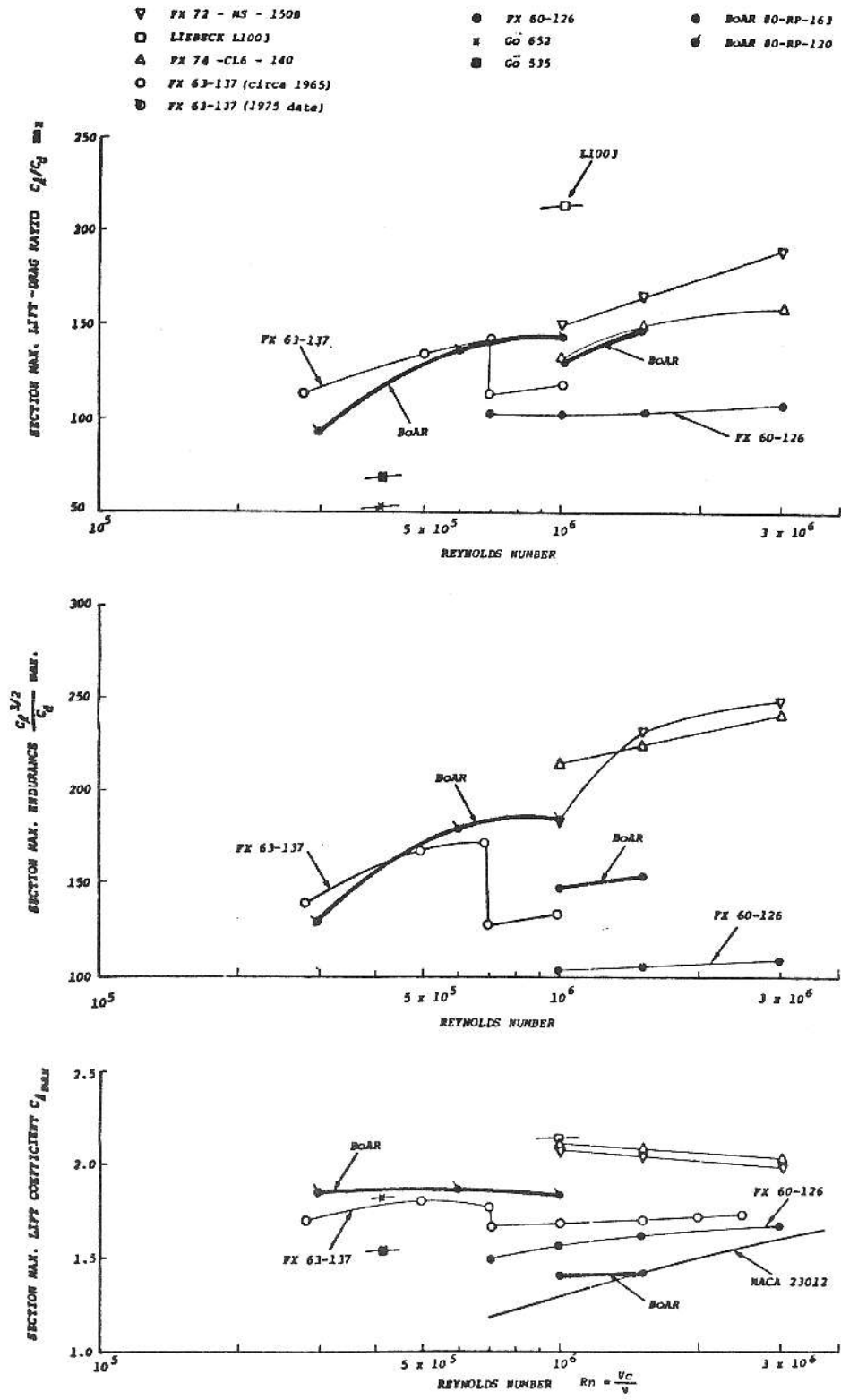


FIGURE 16. PREDICTED PERFORMANCE OF VARIABLE THICKNESS AIRFOIL COMPARED WITH WIND TUNNEL DATA FOR OTHER AIRFOILS AS A FUNCTION OF REYNOLDS NUMBER

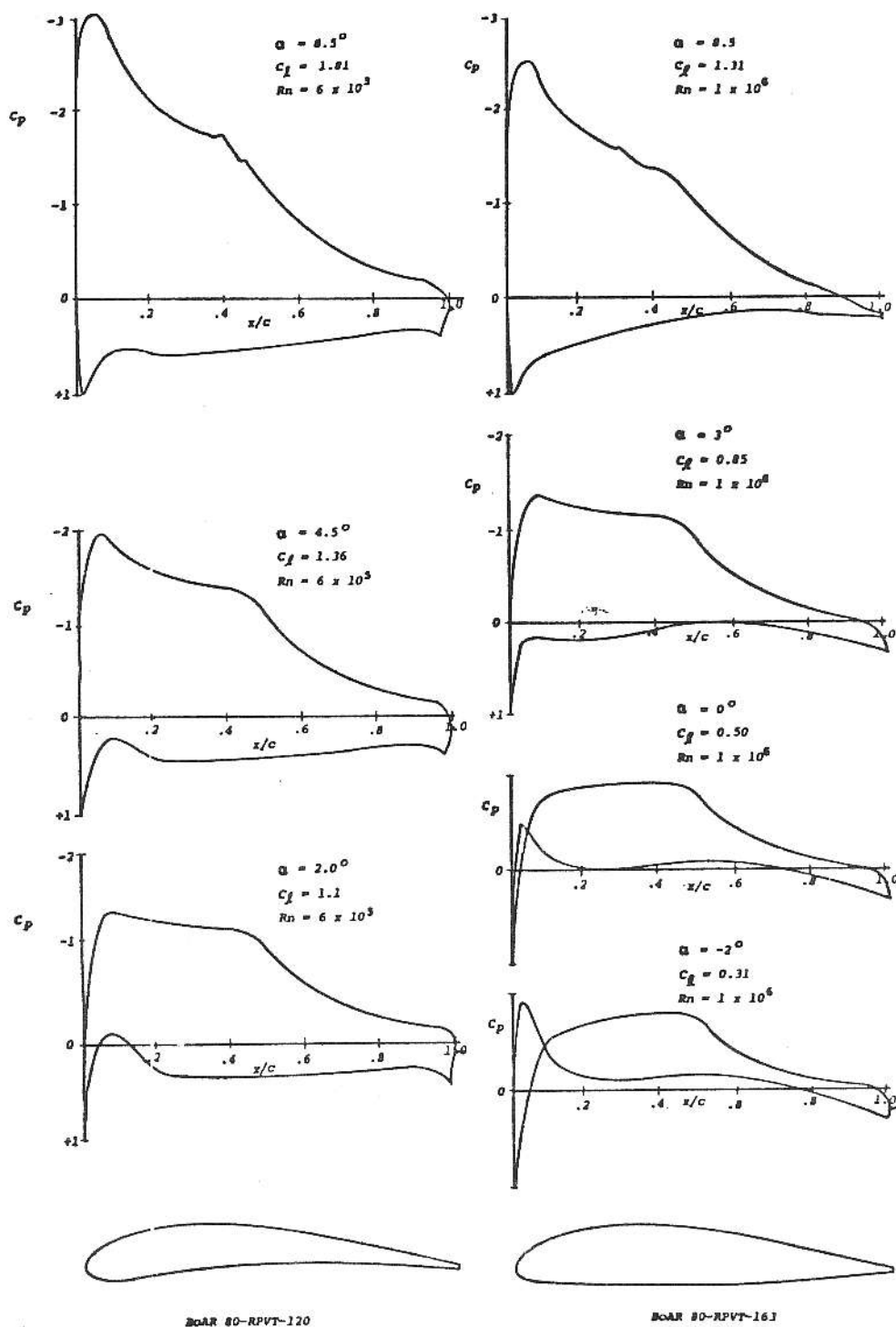


FIGURE 17. THEORETICAL PRESSURE DISTRIBUTION COMPARISON FOR VARIABLE THICKNESS AIRFOILS

Table 3 RP-X Airfoil Design Result

Design Parameter	RP-1/ FX 63-137 Airfoil	RP-X Airfoil Spec.	BoAR 80-RPVT-163 Airfoil	BoAR 80-RPVT-120 Airfoil
1. $c_d = at$ $c_l = 1.0$ $Rn = 10^6$	0.009	0.010	.008	0.009
2. $c_{lmax} = at$ $Rn = 6 \times 10^5$	1.78	2.0	1.4	1.85
3. "High Speed" Drag rise at $c_l \leq$ at $Rn = 1.5 \times 10^6$	Drag creep below $c_l = 0.5$	0.4	0.4	1.0
4. $C_m =$ at $0.4 \leq c_l \leq 1.0$	-0.25	-0.05	-.08 (avg.)	-0.15 (avg.)
5. Stall Characteristics	Gentle	Gentle	Moderate	Sharp
6. Thickness/Chord (t/c_{max} at x/c)	.137 (at $x/c = 0.4$)	.12 (at $x/c = 0.30$)	.163 (at $x/c = 0.35$)	.12 (at $x/c = 0.25$)

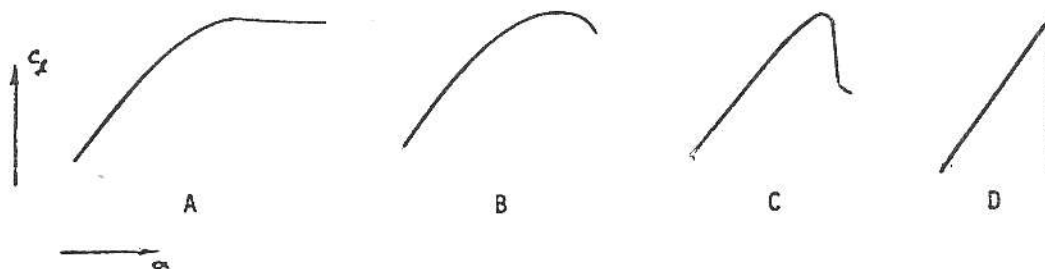
BoAR 80-RPVT-163/120 (Upper Surface)		(Thick and Thin)		BoAR 80-RPVT-163 (Lower Surface)		(Thick)		BoAR 80-RPVT-120 (Lower Surface)		(Thin)	
x/c	x/c	x/c	x/c	x/c	x/c	x/c	y/c	x/c	y/c	x/c	y/c
0	0.0100	0.58168	0.10405	0	+0.0100	0.9600	-0.0015	0	+0.0100	0.8969	+0.0100
0.00008	0.01235	0.60143	0.09995	0.00038	+0.00735	0.9750	-0.0004	0.00038	+0.00735	0.9332	+0.0080
0.00156	0.02048	0.62630	0.09462	0.00122	+0.0035	0.9875	+0.0009	0.00122	+0.0035	0.9600	+0.0060
0.00581	0.02900	0.65134	0.08910	0.00300	0.0000	1.0000	+0.0020	0.00300	0.0000	0.9750	+0.0045
0.01870	0.04554	0.67637	0.08350	0.00380	-0.0013			0.00380	-0.0013	0.9875	+0.0034
0.03094	0.06274	0.70118	0.07791	0.00914	-0.0068			0.00914	-0.0068	1.0000	+0.0020
0.05233	0.07732	0.72619	0.07224	0.01268	-0.0102			0.01268	-0.0102		
0.08312	0.09652	0.75120	0.06656	0.01804	-0.0132			0.01804	-0.0132		
0.10318	0.09387	0.77595	0.06112	0.03000	-0.0181			0.03000	-0.0181		
0.12256	0.09985	0.80091	0.05566	0.03934	-0.0202			0.03934	-0.0202		
0.14289	0.10531	0.82568	0.05029	0.05100	-0.0220			0.05100	-0.0220		
0.16284	0.10931	0.85067	0.04491	0.06830	-0.0232			0.06830	-0.0232		
0.18271	0.11389	0.87567	0.03959	0.09000	-0.0244			0.09000	-0.0231		
0.20267	0.11737	0.90046	0.03425	0.1046	-0.0250			0.1046	-0.0220		
0.22255	0.12033	0.92546	0.02900	0.1300	-0.0257			0.1300	-0.0192		
0.24237	0.12284	0.95041	0.02347	0.1477	-0.0260			0.1477	-0.0150		
0.26224	0.12495	0.97472	0.01730	0.1967	-0.0270			0.1730	-0.0100		
0.28229	0.12670	0.99834	0.01412	0.2510	-0.0285			0.1967	-0.0050		
0.30224	0.12805	1.0000	0.00920	0.3095	-0.0300			0.2380	-0.0000		
0.32213	0.12902			0.3713	-0.0318			0.2510	+0.0020		
0.34205	0.12962			0.4354	-0.0337			0.2750	+0.0050		
0.36195	0.12983			0.5006	-0.0341			0.3095	+0.0095		
0.38185	0.12967			0.5658	-0.0329			0.3713	+0.0140		
0.40180	0.12910			0.6258	-0.0324			0.4354	+0.0180		
0.42171	0.12825			0.6918	-0.0263			0.5006	+0.0220		
0.44167	0.12652			0.7504	-0.0215			0.5658	+0.0230		
0.46172	0.12443			0.8048	-0.0164			0.6258	+0.0220		
0.48172	0.12193			0.8532	-0.0114			0.6918	+0.0210		
0.50153	0.11895			0.8952	-0.0072			0.7504	+0.0190		
0.52142	0.11562			0.9332	-0.0040			0.8048	+0.0150		
0.54143	0.11200							0.8532	+0.0121		
0.56124	0.10820										

TABLE 4. COORDINATES OF THE BoAR 80-RPVT-163/120 VARIABLE THICKNESS AIRFOIL

TABLE 5.
Airfoil Characteristics Comparison

Airfoil	$(t/c)_{max}$ (%)	$c_{l_{max}}$ (@ $Rn =$)	$c_d @ c_l = 1.0$ (@ $Rn =$)	$c_{mc}/4$	Stall Characteristic
Gö 535	16.4	1.55 (4.2×10^5)	0.013 (4.2×10^5)	-0.12	B
Gö 652	17.1	1.83 (4.2×10^5)	0.024 (4.2×10^5)	-0.27	B
FX 60-126	12.6	1.58 (10^6)	0.0102 (10^6)	-0.11	B-C
FX 72-MS-150	15	2.1 (10^6)	0.0102 (10^6)	-0.26	B
FX 74-CL6-14	14	2.1 (10^6)	0.010 (10^6)	n.d.a	C
Liebeck L1003	18	2.15 (10^6)	0.010 (10^6)	-0.03	D

Stall Characteristic Types



CORRIGENDUM

THE FOLLOWING CORRECTIONS SHOULD BE MADE TO THE PAPER "SOME PROBLEMS OF THE DOLPHIN-MODE FLIGHT TECHNIQUE" PUBLISHED IN VOL. VI, NO. 2:

1) Amend W_2 to W_2^* wherever it appears in equations 2, 3, 4, 5 and 6, in the repeti-

tions of these equations on figures 2, 3 and 5 and on the vertical axis on figures 3 and 5.

2) Amend W_1 to $-W_1$ at the left sides of figures 2 and 4.

3) Insert "(where W_2^* is the ratio of climb along L_2)" immediately after equation 2.